Journal of Materials Chemistry B

ROYAL SOCIETY OF CHEMISTRY

COMMUNICATION

View Article Online
View Journal | View Issue

Cite this: *J. Mater. Chem. B*, 2025, **13**, 12895

Received 1st August 2025,
Accepted 22nd September 2025

DOI: 10.1039/d5tb01774b

rsc.li/materials-b

Alternating partially quaternized polytriazole amphiphiles: bridging neutral and ionic domains for tunable aggregation

Anastasiia Hubina, *[a] Yevheniia Lobko,[b] Ivan Khalakhan [b] and Yuliya Khrunyk[c]

Poly(1,2,3-triazole)-based polymers remain underexplored as a versatile platform for biomedical soft materials. Here, we report the modular synthesis of amphiphilic poly(1,2,3-triazole)-*co*-polytriazolium copolymers (qH-PETH) *via* copper(I)-catalyzed azide–alkyne cycloaddition (CuAAC) polyaddition and post-polymerization quaternization with a degree of quaternization equal to (0.85). These polymers exhibit unusual visible colouration in the absence of chromophores—appearing almost colourless in *N*-methyl-2-pyrrolidone (NMP), orange in DMSO, and pale orange in water—accompanied by a pronounced red shift in non-polar solvents such as dichloromethane (DCM) or chloroform. This optical behaviour is attributed to solvent-dependent supramolecular aggregation. Dynamic light scattering (DLS) measurements reveal hydrodynamic diameters of <20 nm in water and approximately 500 nm in chloroform for quaternized polymers (qH-PETH), indicating strong aggregation in low-polarity environments. UV-vis spectroscopy and atomic force microscopy (AFM) further support aggregation-induced optical effects modulated by solvent polarity and hydrogen-bonding capacity. Both neutral and quaternized polymers display excellent cytocompatibility toward human cell lines (HeLa, HEK293, THP-1) at concentrations up to 100 μg mL^{-1}, with no detectable immunogenic activation. These findings position poly(1,2,3-triazole)-*co*-polytriazolium copolymers as a promising, tunable class of biocompatible soft materials for biointerface engineering and responsive biomedical applications.

Introduction

The past two decades have seen a remarkable expansion in the design of stimuli-responsive polymers for biomedical applications. These polymer-based systems are now central to advances in drug delivery, gene transfection, biosensing, imaging, and theranostics,[1] with platforms such as poly(ethylene glycol) (PEG) derivatives,[2] poly(2-oxazoline)s (POx),[3] poly(amino acids),[4] poly(β-uncharged amino esters) (PBAEs), polylactide-based copolymers (*e.g.*, PLGA), and dendrimers (*e.g.*, PAMAM), providing diverse tools for biointerface engineering.[5] Cationic polymers such as polyethylenimine (PEI) remain benchmarks in gene delivery despite well-documented cytotoxicity.[6] Yet across this rich chemical landscape, the design space for multifunctional, supramolecularly active biomedical polymers remains far from fully explored.

1,2,3-Triazole-based polymers are readily accessible *via* copper(I)-catalyzed azide–alkyne cycloaddition (CuAAC) click chemistry and offer an intriguing yet underutilized opportunity.[7,8] The triazole ring combines aromaticity, high dipole moment, hydrogen bonding capacity, and π-stacking propensity, facilitating supramolecular interactions and biological recognition. In small-molecule drug discovery, triazole scaffolds exhibit diverse pharmacological activities, including antifungal, anticancer, antibacterial, anti-inflammatory, and antiviral properties.[3,8–11] At the same time, CuAAC strategy makes it possible to obtain versatile structures, including linear, hyperbranched, and grafted polymers. In polymeric materials, hyperbranched polytriazoles, multiarmed star polytriazoles, and AIE-active polytriazoles have enabled bioimaging, drug encapsulation, and responsive nanostructures.[8,12–14] Yet, compared to other polymer classes, poly(1,2,3-triazole)s remain largely untapped in biomedical materials design.

An even more underexplored class is represented by poly(1,2,3-triazolium)s, ionic derivatives obtained by *N*-alkylation of polytriazoles.[7] These (poly(ionic liquid)s) (PILs) possess tunable solubility, thermal stability, and ionic conductivity, having found their initial applications in electrochemical devices, membranes, and ion conductors. The studies of Drockenmuller *et al.*, reported the substitution pattern of the triazolium ring to modulate ion transport and self-assembly behaviour.[15–20] However, most publications on these polymers focus mainly on their potential as anion-exchange materials and materials for electrochemical and electrochromic applications.[18,21–24] Their potential as biocompatible,

[a] *Department of Polymers, University of Chemistry and Technology Prague, Technická 5, Prague166 28, Czech Republic. E-mail: hubinaa@vscht.cz*
[b] *Department of Surface and Plasma Science, Faculty of Mathematics and Physics, Charles University, V Holešovičkách 2, Prague 180 00, Czech Republic*
[c] *Institute of Biochemistry, Leipzig University, Brüderstraße 34, Leipzig, 04103, Germany*

responsive soft matter is largely unexplored. There are almost no reports on poly(1,2,3-triazolium)s in drug or gene delivery, or biosensing, and the impact of polymer architecture and ionic content on self-assembly has not been investigated. Similarly, there is a lack of systematic evaluations of cytocompatibility, despite growing evidence that low-molecular-weight triazolium compounds exhibit substituent-dependent biological responses.[25,26]

In this work, we present a new amphiphilic single-chain poly(1,2,3-triazole) polymer and its quaternized derivative poly (1,2,3-triazole)-*co*-polytriazolium, synthesized *via* CuAAC polyaddition of PEG1000-diyne and 1,6-diazidohexane segments, followed by postpolymerization *N*-alkylation. These polymers exhibit solvent-induced aggregation and visible solvatochromism without added dyes, arising from emergent supramolecular ordering. Dynamic light scattering (DLS), UV-vis spectroscopy, and atomic force microscopy (AFM) confirm the formation of solvent-tunable nanostructures, accompanied by a visible colour change. Critically, both the neutral and partially quaternized polytriazoles display no detectable cytotoxicity in HeLa, HEK293, and THP-1 cell lines, even at high polymer concentrations (up to 100 μg mL^{-1}), and show no apparent immunogenic response. These results demonstrate that simple, scalable triazole chemistry followed by straightforward postpolymerization modification can yield biocompatible, optically responsive polymers with supramolecular activity. This approach could be used to design new materials for sensing, imaging, and active interfaces in soft matter and biomedicine.

Experimental

Materials

Polyethylene glycol 1000 (PEG1000) ($M_n \approx 1000$ g mol^{-1}), 1, 6-dichlorohexane, ascorbic acid, propargyl bromide (80% in toluene), sodium azide and 1-bromohexane were purchased from Sigma Aldrich (Germany), sodium hydroxide, copper(II) sulphate pentahydrate, hydrochloric acid (35%), magnesium sulphate (anhydrous), and all solvents (reagent grade) were purchased from Penta (Czech Republic) and used as received unless otherwise noted. Sodium ascorbate was prepared freshly before use by neutralizing ascorbic acid with equimolar sodium hydroxide in distilled water.

Methods

^{1}H NMR spectra were recorded using a 500 MHz Bruker Avance 500 spectrometer in $CDCl_3$ or DMSO-d_6 at 25 °C. FTIR spectra were recorded with the help of Nicolet 6700 FTIR-spectrometer (Thermo-Nicolet) in the ATR mode (wavenumber range of 4000–600 cm^{-1}). Gel permeation chromatography (GPC) was performed using Waters SEC-RI chromatograph (Waters 515 pump, Waters 2414 refractive index detector, ECOM 4 channel degasser). Separation of polymers (~1 mg mL^{-1} solution in DMF (0.1 M LiBr)) was done at 35 °C on linear column (7.8 × 300 mm) using DMF (0.1 M LiBr) as mobile phase (0.8 mL min^{-1}). UV-vis absorption spectra were recorded at room temperature in quartz cuvettes (1 cm path length) across various solvents and solvent mixtures with constant concentrations of the polymer, either 0.75 mg mL^{-1} or 1 mg mL^{-1}, using spectrophotometer Cary 50 (Varian) in the wavelength range 200–800 nm. Dynamic light scattering (DLS) measurements were conducted on Zetasizer Pro (Malvern, USA) in quartz cuvettes (1 cm path length) across various solvents and solvent mixtures with constant concentrations of the polymer, either 0.75 mg mL^{-1} or 1 mg mL^{-1}, at RT without any pretreatment. For AFM imaging, polymer solutions (0.25 mg mL^{-1}) were prepared in the respective solvents or solvent mixtures, drop-cast onto cleaned silicon wafer substrates, and allowed to dry slowly at room temperature under ambient conditions. The dried films were imaged in tapping mode under ambient atmosphere with Bruker MultiMode 8 AFM using ScanAsyst-Air probes (Bruker). Acquired images were processed using NanoScope 1.9 software (Bruker).

Cell cultures. Human embryonic kidney (HEK) 293 cells were cultured in Dulbecco's modified Eagle's medium (DMEM)/Ham's F12 (1 : 1) (Lonza, Basel, Switzerland) supplemented with 15% fetal bovine serum (FBS) (Biochrom GmbH, Berlin, Germany). Human cervix carcinoma (HeLa) cells were cultured in RPMI 1640 (Lonza) supplemented with 10% FBS. A suspension cell line THP-1 was cultured in RPMI 1640 (10% FBS and 10 mM glutamine, Lonza). All cells were maintained in T75 cell culture flasks at 37 °C, 95% humidity, and 5% CO_2 (standard conditions). These cell lines were used for no more than 15 passages. Medium was changed every 4–5 days.

Mitochondrial activity assay by resazurin conversion

Mitochondrial activity of cells was evaluated by a resazurin conversion assay.[27,28] Briefly, cells (15 000/well), seeded into 96-well cell culture plates (*i.e.* THP-1 in Greiner (Kremsmünster, Austria) with non-binding surfaces, HeLa and HEK293 in TPP (Trasadingen, Switzerland)), were cultured in respective media containing tested compounds in various concentrations: 0, 0.78, 1.56, 3.125, 6.25, 12.5, 25, 50, and 100 μg mL^{-1}. Following 24 h of incubation, cell culture medium was aspirated, cells were rinsed with PBS, and further incubated with 100 μL of a sterile resazurin solution (0.0025% in PBS) (Sigma-Aldrich, St. Louis, MO, USA) at 37 °C. In parallel, aiming to evaluate the viability of a total amount of THP-1 cells (*i.e.*, adhered and non-adhered), resazurin solution (100 μL) was added directly to the cell suspension. THP-1 cells induced by phorbol 12-myristate 13-acetate (PMA, Thermo Fischer Scientific (Ward Hill, MA, USA), 200 nM) were used as a positive control. The resulting fluorescence (excitation λ: 550 nm, emission λ: 595 nm) was measured using a Tecan Spark multimode microplate reader (Tecan Group, Männedorf, Switzerland) after incubation for 30 min, 60 min, 90 min, and 120 min. Blank values obtained for the respective conditions without cells were subtracted from the obtained fluorescence data.

Syntheses

Synthesis of PEG1000-diyne

PEG1000 (5.00 g, ~5.00 mmol, $M_n \approx 1000$ g mol^{-1}) was dissolved in 50 mL of anhydrous THF and dried by argon bubbling for 1 hour. A dispersion of sodium hydride (0.24 g, 10.0 mmol,

2.0 equivalents, 60% in mineral oil) in THF was added dropwise over 20 minutes under argon at room temperature. The reaction mixture was stirred for an additional 1 hour. Propargyl bromide (1.00 mL, ~12.0 mmol, 2.4 equivalents, 80% in toluene) was then added slowly, and the solution was stirred at 60 °C for 17 hours. After cooling to room temperature, 20 mL of 4% aqueous HCl was added slowly to quench excess sodium hydride. The reaction mixture was concentrated under reduced pressure to remove THF, and the residue was extracted with dichloromethane (3 × 30 mL). The solution was washed with brine, and residual water was removed first in a separation funnel and then by drying over anhydrous magnesium sulfate. The solvent was removed under vacuum to yield a pale viscous product, which solidified upon storage at 2 °C. The PEG1000-diyne was used directly in polymerization without further purification (4.2 g, yield 80%). ^{1}H NMR (500 MHz, $CDCl_3$) δ (ppm): 4.23 (d, 4H, HC≡C-C**H$_2$**-), 3.74–3.60 (m, 88H, -O-C**H$_2$**-C**H$_2$**-), 2.47 (t, 2H, **H**C≡C-CH$_2$-), (Fig. S1A).

Synthesis of 1,6-diazidohexane

1,6-Dichlorohexane (5.00 g, ~30.8 mmol) was dissolved in 75 mL of THF, and sodium azide (4.86 g, ~74.0 mmol, 2.4 equivalents) was added. The reaction mixture was refluxed at 70 °C for 24 hours under ambient atmosphere. After cooling to room temperature, the mixture was washed sequentially with 4% aqueous HCl and distilled water. The organic layer was separated using a separatory funnel, dried over anhydrous magnesium sulfate, filtered, and concentrated under reduced pressure. The product was obtained as a colourless to pale yellow transparent oil and used directly in polymerization without further purification (3.0 g, yield 88%). ^{1}H NMR (500 MHz, $CDCl_3$) δ (ppm): 3.31(t, 4H, N_3-C**H$_2$**-), 1.6 (p, 4H, N_3-CH$_2$-C**H$_2$**-), 1.45 (m, 4H, N_3-CH$_2$-CH$_2$-C**H$_2$**-), (Fig. S1B).

Synthesis of poly(PEG1000-triazole-hexyl) (PETH)

A step-growth click polyaddition was carried out under ambient conditions without inert atmosphere or pretreatment of solvents. PEG1000-diyne (approximately 2.00 g, ~2.00 mmol) and 1,6-diazidohexane (~0.41 g, ~2.00 mmol) were dissolved in 75 mL of reagent-grade DMF. Sodium ascorbate (0.10 g, ~0.50 mmol) was dissolved in 2 mL of distilled water and added to the reaction mixture under stirring. After 10 minutes, an aqueous solution of $CuSO_4{\cdot}5H_2O$ (0.025 g, ~0.10 mmol in 2 mL water) was added dropwise. The reaction was stirred at room temperature for 24 hours. The crude reaction mixture was extracted three times with dichloromethane. The organic layer was washed sequentially with 4% aqueous HCl and distilled water (3×), then dried over anhydrous magnesium sulfate. The solvent was removed under reduced pressure. The resulting residue was redissolved in DMF and precipitated into cold diethyl ether. This redissolution–reprecipitation cycle was repeated three times. The final product was dried under vacuum overnight at 40 °C to yield the polymer as a dark brown solid (1.8 g, yield 74%). ^{1}H NMR (500 MHz, DMSO) δ (ppm): 8.06 (s, 1H, triazole ring), 4.49 (s, 4H, triazole-C**H$_2$**-O-CH$_2$-CH$_2$-), 4.3 (t, 4H, triazole-C**H$_2$**-CH$_2$-CH$_2$-), 4.1 (d, 4H, HC≡C-C**H$_2$**-), 3.59–3.39 (m, 88H, -O-C**H$_2$**-C**H$_2$**-), 1.77 (s, 4H triazole-CH$_2$-C**H$_2$**-CH$_2$-), 1.27 (s 4H triazole-CH$_2$-CH$_2$-C**H$_2$**-), (Fig. S1C).

The synthesized PETH polymer, as characterized by SEC, exhibited an apparent number-average molecular weight (M_n) of approximately 9900 g mol^{-1} and a weight-average molecular weight (M_w) of 14 000 g mol^{-1}, indicating a moderate molecular weight distribution (D =1.42) consistent with step-growth polyaddition (SI Fig. S3).

Quaternization of polytriazole qH-PETH

The neutral PETH (0.50 g, estimated ~1.0 mmol triazole units) was dissolved in 10 mL of DMF, and 1-bromohexane (3.7 mL, ~20 mmol, 20 equivalents relative to triazole) was added directly. The reaction mixture was stirred at 80 °C for 48 hours under ambient atmosphere. After cooling, the reaction mixture was poured into excess cold diethyl ether. The precipitated polymer was collected by centrifugation and washed with ether. This precipitation cycle was repeated three times, or until the supernatant became completely transparent. The final product was dried under vacuum at 40 °C overnight, affording the partially quaternized poly(1,2,3-triazolium) bromide as a dark orange, sticky polymer (0.39 g, yield 73%). ^{1}H NMR (500 MHz, DMSO) δ (ppm): 9.95 (s, 1H triazolium) 8.06 (s, 1H, triazole), 4.85 (s, 4H, triazolium-C**H$_2$**-O-CH$_2$-CH$_2$-), 4.58 (t, 4H, triazolium, -C**H$_2$**-CH$_2$-CH$_2$-, 2H, triazolium-C**H$_2$hexyl**), 4.51 (s, 4H, triazole-C**H$_2$**-O-CH$_2$-CH$_2$-), 4.3 (t, 4H, triazole-C**H$_2$**-CH$_2$-CH$_2$-), 4.15 (d, 4H, HC≡C-C**H$_2$**-), 3.68–3.4 (m, 88H, -O-CH$_2$-C**H$_2$**-), 1.9 (m, 4H triazole-CH$_2$-C**H$_2$**-CH$_2$-, 8H, triazolium-CH$_2$-(C**H$_2$**)$_4$-CH$_3$), 1.2 (s 4H triazole-CH$_2$-CH$_2$-C**H$_2$**-), 0.8 (m, 3H, triazolium-CH$_2$-(CH$_2$)$_4$-C**H$_3$**) (Fig. S1D).

The degree of quaternization was calculated from ^{1}H NMR spectrum of qH-PETH (SI Fig. S1D) as follows: DQ = $(I_{c'})/(I_c + I_{c'})$, where c′ is proton in triazolium ring and c is a proton in triazole ring. Calculated DQ is 0.85.

Results and discussion

Both PETH and qH-PETH polymers do not incorporate classical chromophores or extended π-conjugation (Scheme 1). Nevertheless, the solutions of these polymers exhibit distinct visible coloration in certain solvents, suggesting that the optical response arises from supramolecular interactions rather than intrinsic electronic transitions. This points toward an aggregation-induced solvatochromism (AIS) mechanism, where solvent-dependent self-assembly modulates the local electronic environment of the polymer chains. AIS is reported for other types of polymers, such as polythiophenes[29,30] and polydiacetylenes,[31] as well as for nonconjugated polymers such as poly[(maleic anhydride)-*alt*-(vinyl acetate)],[32] but up to our knowledge was not demonstrated either for polytriazoles or polytriazoliums. To elucidate this behaviour, we systematically investigated how solvent polarity and hydrogen-bonding capacity influence both the aggregation state and the observed colour change. In addition, the biocompatibility of the

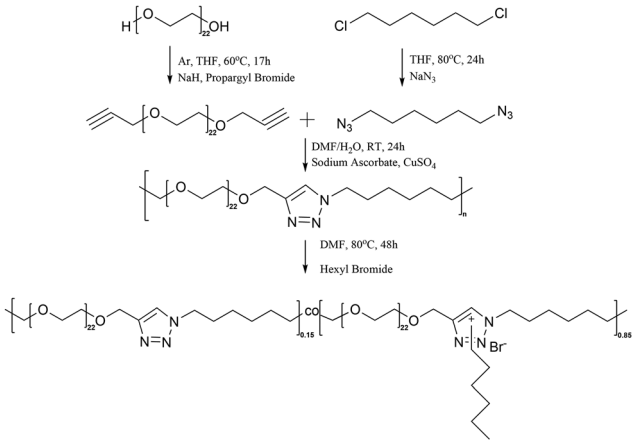

Scheme 1 Synthesis of α,ω-PEG1000-dyine, 1,6-diazidohexane, poly (ethylene glycole-triazole-hexyl) (PETH), partially hexyl-quaternized poly(ethylene glycole-triazole-hexyl) (qH-PETH).

polymers was assessed to evaluate their suitability for prospective biomedical applications.

Visual solvatochromism across solvent polarity

A comparative visual analysis of polymer solutions (Fig. 1) reveals distinct solvatochromic behaviour of both neutral PETH and its quaternized analogue qH-PETH.

In solvents such as DMSO, acetone, and acetonitrile, qH-PETH shows a rich orange hue (absorbance at ~512 nm), indicative of self-assembly-driven chromophore-like behaviour. This behaviour is likely due to interactions between triazolium moieties and their hydrophobic tails. In contrast, in highly polar and strongly solvating media *e.g.* NMP and water, the solutions appear almost colourless (weak absorbance at 485 nm in NMP), suggesting good solvation of the polymer chains and the disruption of the aggregation responsible for solvatochromism. While in water H-bonding leads to formation of nanoparticles ~10 nm size and absorption peak at (476 nm).

The neutral polymer PETH, by comparison, shows more uniform and less intense colouration across all solvents, supporting the idea that ionic character and amphiphilic structure in qH-PETH amplify its solvent-responsive behaviour. These visual trends are consistent with spectroscopic data (Fig. 1(C) and (D)) and point toward solvent-mediated morphological changes as the key mechanism behind the observed solvatochromism.

The aqueous solutions of qH-PETH are of particular interest for potential biomedical applications; therefore, we investigated their colloidal stability across a relevant concentration range. Dynamic light scattering and UV-vis spectroscopy revealed that between 0.25 and 1.0 mg mL^{-1}, both the particle size and absorption maximum remained unchanged, indicating robust aggregation behaviour (Fig S6). Furthermore, time-dependent studies demonstrated excellent stability, particle size did not demonstrate significant change after 48 h, with the results corroborated by a consistent zeta potential modulus of approximately 40 mV (Fig. S7).

Aggregation behaviour explained by Kamlet–Taft parameters of the solvents

The dependence of polymer aggregate size on solvent properties was systematically investigated by correlating the measured hydrodynamic diameters from dynamic light scattering (DLS) with the Kamlet–Taft parameters of the solvents used: α (hydrogen-bond donor acidity), β (hydrogen-bond acceptor basicity), and π* (dipolarity/polarizability).[33] The contour maps (Fig. 2) reveal clear trends in how these solvent parameters influence the extent of self-assembly of both polymers.

The dependence of aggregate size of the neutral polymer PETH on solvent properties is illustrated in the contour plots correlating particle size (all the DLS data is available in the SI). Fig. 2 shows the Kamlet–Taft parameters α (HBD) (Fig. 2A), β (HBA) (Fig. 2B), and π* (dipolarity/polarizability). In this case, aggregate formation does not correlate simply with solvent polarity: while relatively small particles are observed in moderately polar aprotic solvents such as acetone, ACN, and THF, the largest aggregate sizes occur in highly polar and strongly hydrogen-bonding solvents such as NMP and water. This suggests that hydrogen bonding and polymer–polymer association dominate

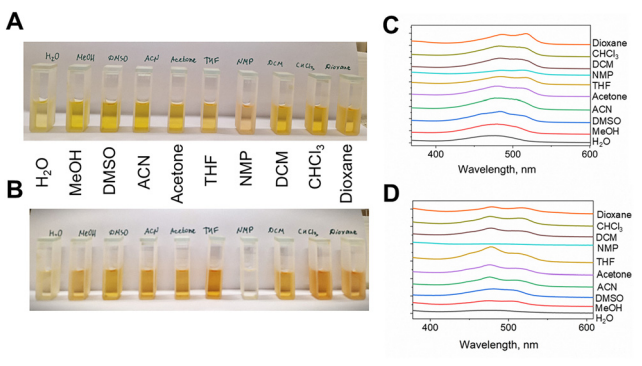

Fig. 1 Solvent-dependent colour change of PETH (A) and qH-PETH (B) solutions in selected solvents at identical concentration (0.75 mg mL^{-1}) and UV-vis absorbance spectra of PETH (C) and qH-PETH (D) in different solvents.

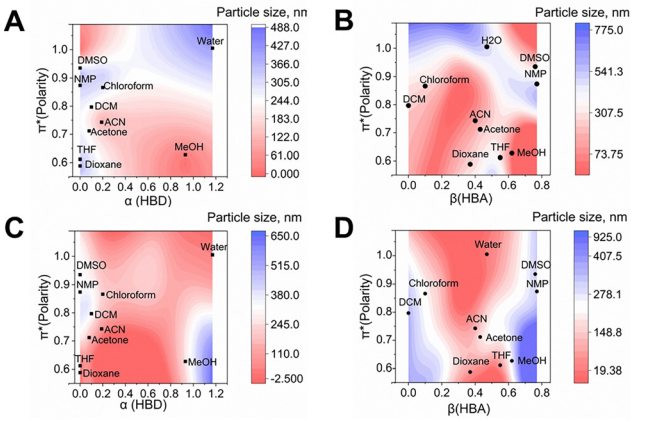

Fig. 2 Contour plots of polymer particles size correlation with Kamlet–Taft parameters of the solvents of PETH (A) and (B) and qH-PETH (C) and (D).

in these environments, possibly due to partial desolvation of hydrophobic domains and promotion of interchain interactions through hydrogen bonding networks. In contrast, in low polarity, weakly hydrogen-bonding solvents (DCM, chloroform), moderate to large aggregates also form through hydrophobic-driven self-assembly. Overall, the behaviour of the neutral polymer reflects a complex balance between polarity and hydrogen-bonding effects, rather than a simple polarity-driven solubility trend.

For the charged polymer qH-PETH, the aggregation behaviour exhibits a more systematic dependence on solvent polarity. As seen in the contour plots, the particle size increases progressively along the solvent polarity sequence: dioxane < THF < acetone < ACN < NMP < DMSO, demonstrating that increased polarity promotes interchain interactions and aggregation in these aprotic solvents. This trend likely reflects the decreased ability of aprotic polar solvents to fully shield the ionic groups and hydrophobic segments simultaneously, favouring associative interactions. However, in water, the behaviour is strikingly different: extremely small particles are formed, suggesting the presence of highly solvated, potentially single-chain particles stabilized by strong hydrogen bonding with the aqueous environment. This distinct behaviour highlights the critical role of hydrogen-bond donor capacity (α) in promoting molecular dispersion of the charged polymer in water, being in sharp contrast to its aggregation tendency in polar aprotic solvents.

In conclusion, while the neutral polymer PETH exhibits a complex aggregation pattern influenced by both hydrophobic interactions and hydrogen bonding, the charged polymer shows a clear polarity-dependent aggregation trend in aprotic solvents, with water uniquely favouring molecular dispersion. This illustrates how charge and solvation effects fundamentally alter the self-assembly landscape of two polymer systems.

To clarify the influence of both polarizability and H-bonding, we prepared two series of qH-PETH sample in water mixed with other solvent in various ratios, first with DMSO considering that two solvents have close polarity but extremely different proton donating ability (HBD) (Fig. 3). The dual-axis plot illustrating particle size and absorption maximum (λ_{max}) in DMSO/water mixtures reveal a strong correlation between aggregation and solvatochromic behaviour, governed by the solvent environment's Kamlet–Taft parameters. As the DMSO content increases (*i.e.*, α decreases and β increases), the particle size rises sharply, indicating enhanced aggregation. This trend reflects the poor hydrogen bond donor (HBD) capacity of DMSO (α = 0.00), which fails to stabilize the charged and hydrophilic segments of the polymer, thus promoting interpolymer interactions and self-assembly. Concurrently, the absorption maximum undergoes a redshift, consistent with the formation of larger, more ordered aggregates which suggest that solvatochromism is aggregation-induced. In contrast, high water content (α = 1.17, β = 0.47) leads to minimal aggregation and a blue-shifted λ_{max}, pointing to the presence of molecularly dispersed chains in a strongly hydrogen-bonding medium. These findings demonstrate that solvent polarity and hydrogen-bonding parameters, especially α, critically govern both the size and optical response of the polymer assemblies.

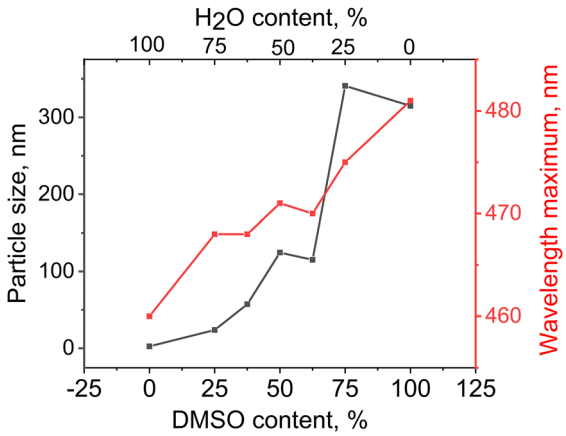

Fig. 3 Dependence of particle size (black) and UV-vis absorption maximum (red) of the qH-PETH in DMSO/water mixtures (0.25 mg mL^{-1}).

These observations were further supported by AFM images of the samples prepared from the same solutions (Fig. 4). In water and in mixtures with higher water content, qH-PETH forms nanoparticles, probably single-chain. As the water content decreases as well as α (α_{H_2O} = 1.17, α_{DMSO} = 0), the biggest aggregates, probably micelle-like, are formed mainly due to hydrophilic–hydrophobic interactions.

These results suggest that by tuning solvent polarity and hydrogen-bond donor capacity, it is possible to control the transition between discrete, molecularly dispersed chains and self-assembled aggregates of the charged polymer. Such control over aggregation behaviour could be further explored for designing systems where triggered disassembly or size modulation is desirable, for example, in intracellular delivery or responsive release formulations.

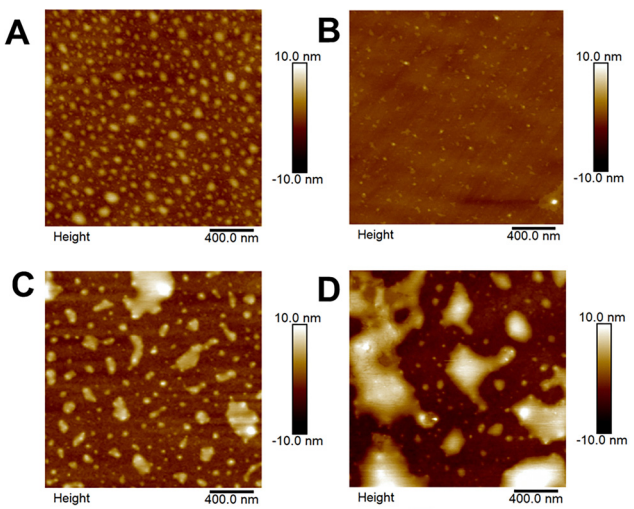

Fig. 4 AFM images of qH-PETH solutions (0.25 mg mL^{-1}) in DMSO/water mixtures: A – 0/100; B – 25/75; C – 50 : 50; D – 75/25.

Influence of the solvents on aggregation behaviour and morphology

Building on the solvent-dependent behaviour observed in DMSO/water mixtures, a complementary comparison between pure water and dioxane further highlights the critical role of solvent polarity and hydrogen-bonding capacity in modulating qH-PETH assembly and optical response. Fig. 4A illustrates the pronounced solvent-dependent behaviour of qH-PETH in water *versus* dioxane, demonstrating clear differences in optical properties, aggregation, and morphology. Visually, the polymer solution in dioxane appears deep orange, while in water it remains pale orange, indicating solvatochromic behaviour. This was confirmed by UV-vis absorbance spectra (centre left), where the dioxane sample shows a broad absorbance peak around 480–500 nm, consistent with aggregation-induced spectral features, whereas the water sample exhibits lower and flatter absorbance. Dynamic light scattering (centre right) reveals a stark contrast in particle sizes: in water, the polymer forms very small assemblies (<10–20 nm), while in dioxane, large aggregates ranging from 600 to over 1200 nm dominate the volume distribution, suggesting hydrophobic-driven aggregation and further precipitation (observed in 48 h) in the aprotic solvent. Corresponding AFM images (Fig. 5) support this interpretation. In water, nanoscale spherical features are visible and distributed across the surface, indicating stable, dispersed nanostructures, while in dioxane, a smooth, film-like morphology without discrete features reflects the presence of collapsed or fused polymer aggregates. Together, these results confirm that qH-PETH undergoes solvent-driven reorganization, transitioning from electrostatically stabilized nanostructures in polar protic media to large, disordered aggregates in low-polarity solvents.

According to AFM images of the water/dioxane mixtures (Fig. 6), the self-assembly follows a distinct path. The polymer is well-dissolved in pure dioxane, forming a smooth polymer film, no aggregation is also observed at 75% dioxane content. As water content increases, particle-like features begin to appear, with the most pronounced and uniformly distributed spherical assemblies emerging at 100% water.

This difference in aggregation behaviour, compared to DMSO/water systems, reflects the solvent's ability to mediate intermolecular interactions. Dioxane, being less polar and less

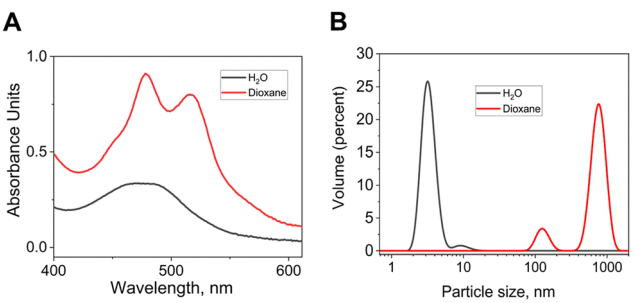

Fig. 5 qH-PETH solutions in water and dioxane: A – UV-vis spectra, B – particle size distribution according to DLS.

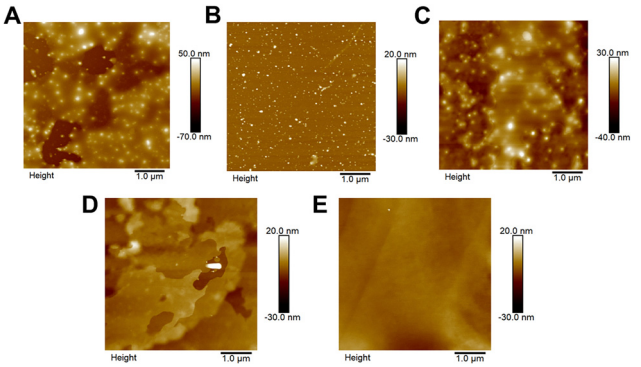

Fig. 6 AFM images of qH-PETH solutions (0.185 mg mL^{-1}) in water/dioxane mixtures: A – 100/0; B – 75/25; C – 50 : 50; D – 25/75; E– 0/100.

hydrogen-bonding than DMSO, facilitates sharper transitions in morphology upon water addition. These findings further demonstrate the polymer's sensitive and tunable self-assembly profile driven by solvent polarity and hydrogen-bonding capacity, supporting the potential of qH-PETH as a responsive nanomaterial platform.

In both DMSO/water and dioxane/water solvent systems, DLS measurements reveal a progressive decrease in particle size as the water content increases, consistent with a transition from a molecularly dissolved state to well-defined nanostructures.

Although the polymer lacks conventional chromophores, UV-vis spectra still show notable changes in the visible region with solvent composition. These subtle spectral shifts and intensity changes are most likely due to aggregation-induced modulation of the electronic environment, for instance, alterations in local dielectric constant, dipole orientation, or short-range packing between quaternized triazolium groups and surrounding PEG segments. The intensity increase in more aqueous conditions aligns with the formation of ordered aggregates, as observed by AFM and supported by DLS.

Effect of PETH and qH-PETH on the viability of tumour and non-tumour cells

Beyond tunable self-assembly behaviour, the suitability of these polymers for biomedical applications critically depends on their cytocompatibility. We therefore evaluated the effects of both neutral and quaternized polymers on the viability of representative human cell lines, using a resazurin-based assay across a range of polymer concentrations.

After 24 hours of cultivation, the mitochondrial activities of cells incubated with tested compounds were analyzed by resazurin conversion to resorufin (Fig. 7 and 8). To test an immunogenic and/or allergenic potential of PETH and qH-PETH, THP-1 suspension cells (the human leukaemia monocytic cell line) were employed as a model of monocyte-to-macrophage differentiation.[28] After incubation with various concentrations of PETH and of qH-PETH, THP-1 cell suspension was aspirated to detect the viability of only adhered cells (Fig. 7A and 8A). THP-1, exposed to PMA, which induces a rapid cell adhesion and their differentiation into cells with a macrophage-like

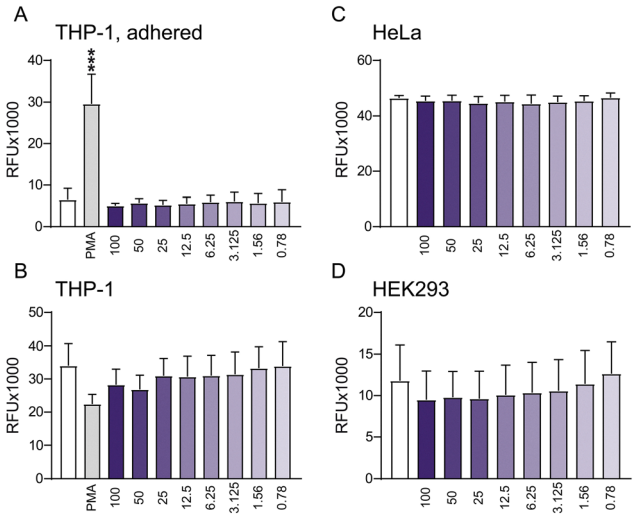

Fig. 7 Summary of the results of resazurin reduction in cell cultures: THP-1 (adhered (A), adhered and non-adhered (B)), HeLa (C), and HEK293 (D) at 24 h after incubating cells with PETH. The levels of relative fluorescence units (RFU) are shown for cells cultured in media containing no PETH (white colour) and PETH in different concentrations, *i.e.* 100, 50, 25, 12.5, 6.25, 3.125, 1.56, 0.78 μg mL^{-1} (shades of violet). RFU results for THP-1 cells induced by PMA (200 nM) are shown in grey. The measurements were taken at 120 min following incubation with resazurin. Data (represented as mean ± SEM; n = 3) were analyzed by one-way ANOVA followed by Tukey's *post hoc* test; in (A), PMA-stimulated THP-1 cells showed significantly higher responses compared to untreated cells and cells cultured in medium supplemented with PETH at all tested concentrations ($p < 0.001$, shown by ***). In panels (B–D), no statistically significant differences were observed between the tested conditions.

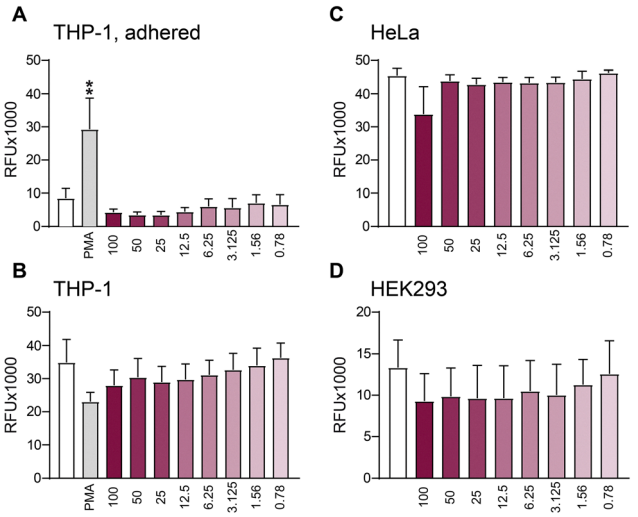

Fig. 8 Summary of the results of resazurin reduction in cell cultures: THP-1 (adhered (A), adhered and non-adhered (B)), HeLa (C), and HEK293 (D) at 24 h after incubating cells with qH-PETH. The levels of relative fluorescence units (RFU) are shown for cells cultured in media containing no qH-PETH (white colour) and qH-PETH in different concentrations, *i.e.* 100, 50, 25, 12.5, 6.25, 3.125, 1.56, 0.78 μg mL^{-1} (shades of dark cherry). RFU results for THP-1 cells induced by PMA (200 nM) are shown in grey. The measurements were taken at 120 min following incubation with resazurin. Data (represented as mean ± SEM; n = 3) were analyzed by One-Way ANOVA followed by Tukey's *post hoc* test; in (A), PMA-stimulated THP-1 cells showed significantly higher responses compared to cells cultured in medium supplemented with qH-PETH at all tested concentrations ($p < 0.01$, shown by **). In addition, PMA-stimulated THP-1 cells differed significantly from untreated THP-1 cells ($p < 0.05$). In panels (B–D), no statistically significant differences were observed between the tested conditions.

phenotype,[28] were used as a positive control. In contrast to a positive control showing dramatically elevated levels of RFU (Fig. 7A and 8A), for all PETH and qH-PETH concentrations tested, no increase in adhered THP-1 cells was detected, and the observed RFU levels were comparable to those for untreated cells. Furthermore, the range of concentrations of both compounds used for this assay did not induce cytotoxicity in THP-1, as was shown by a resazurin reduction of both adhered and non-adhered cells (Fig. 7B and 8B). The results indicate that PETH and qH-PETH (at the tested concentrations) might not induce a mono-;cyte recruitment and their subsequent activation into macrophages.

Potential cytotoxic effects of PETH and qH-PETH were further tested employing human cervical cancer cell line HeLa (Fig. 7C and 8C) and a human embryonic kidney cell line HEK293 (Fig. 7D and 8D). To data obtained for HeLa, no toxic impact on cell viability was observed for PETH up to its highest concentration used (100 μg mL^{-1}, Fig. 7C). The same concentration of qH-PETH resulted in a decreased RFU level of HeLa, but not to a significant level. All the other concentrations of qH-PETH tested, however, did not affect HeLa cell viability (Fig. 8C). Both compounds, PETH and qH-PETH, tended to slightly reduce HEK293 viability in a concentration-dependent manner (Fig. 7D and 8D), but not to a significant level.

Conclusions

While several prior studies have explored polytriazole-based materials in biomedical and optical contexts, the present research proposes a new application of robust CuAAC polyaddition with subsequent quaternization as a path to obtain amphiphilic poly(1,2,3-triazole)-*co*-poly(triazoliums)s for potential biomedical applications. To our knowledge, no previous study has reported single-chain amphiphilic poly(1,2,3-triazole)-*co*-poly(triazolium) copolymers that exhibit intrinsic solvatochromism arising from solvent-responsive self-assembly, without requiring embedded chromophores or metal complexes. In this research, we synthesised poly(PEG1000-triazole-hexane)-*co*-(PEG1000-triazolium-hexane)hexyl *via* straightforward CuAAC polyaddition followed by postpolymerization quaternization. Both the neutral and partially quatrnized polytriazole were shown to undergo self-assembly and demonstrate self-assembly induced solvatochromic behaviour, as well as responsiveness to the changes in media polarity and H-bonding capacity in the solvent mixtures (water *vs.* DMSO and water *vs.* dioxane). AFM imaging confirmed this trend, as well as, combined with DLS measurements confirmed that alternating partially charged polytriazole is able to form nanoparticles in water dispersions. Additionally, both neutral and quaternized polymers demonstrated

excellent cytocompatibility toward human cell lines (HeLa, HEK293, THP-1) up to 100 μg mL^{-1}, with no apparent immunogenic activation.

Thus, the systematic analysis of solvents' effects using Kamlet–Taft parameters, together with direct visualization by AFM and a demonstration of excellent cytocompatibility, positions this class of polymers as highly promising platform for the development of responsive biointerfaces and sensing materials. These findings essentially expand the functional scope of polytriazole-based polymers beyond their current applications, establishing a new modular design paradigm for stimuli-adaptive soft materials.

Author contributions

Anastasiia Hubina – conceptualization, visualization, methodology, investigation, writing – original draft, writing – review & editing, Yevheniia Lobko – investigation, writing – review & editing, Ivan Khalakhan –investigation, writing – review & editing, Yuliya Khrunyk– investigation, methodology, writing – review & editing.

Conflicts of interest

There are no conflicts to declare.

Data availability

The data supporting this article have been included as part of the supplementary information (SI). Supplementary information is available. See DOI: **https://doi.org/10.1039/d5tb01774b**.

Notes and references

1 B. T. Luk and L. Zhang, *ACS Appl. Mater. Interfaces*, 2014, **6**(24), 21859–21873.
2 D. Hutanu, M. Frishberg, L. Guo and C. Darie, *Mod. Chem. Appl.*, 2014, **2**, 1–6.
3 R. Luxenhofer, Y. Han, A. Schulz, J. Tong, Z. He, A. V. Kabanov and R. Jordan, *Macromol. Rapid Commun.*, 2012, 1613–1631.
4 M. Khuphe and P. D. Thornton, *Eng. Biomater. Drug Delivery Syst.*, 2018, 199–228.
5 K. Hori, S. Yoshimoto, T. Yoshino, T. Zako, G. Hirao, S. Fujita, C. Nakamura, A. Yamagishi and N. Kamiya, *J. Biosci. Bioeng.*, 2022, **3**, 195–207.
6 F. A. De Oliveira, L. J. C. Albuquerque, G. Delecourt, V. Bennevault, P. Guégan and F. C. Giacomelli, *Curr. Gene Ther.*, 2021, 431–451.
7 M. M. Obadia and E. Drockenmuller, *Chem. Commun.*, 2016, **52**, 2433–2450.
8 J. F. Lutz and Z. Zarafshani, *Adv. Drug Delivery Rev.*, 2008, 958–970.
9 C.-H. Zhou and Y. Wang, *Curr. Med. Chem.*, 2012, 239–280.
10 R. Kharb, P. C. Sharma and M. S. Yar, *J. Enzyme Inhib. Med. Chem.*, 2011, **26**, 1–21.
11 A. Massarotti, S. Aprile, V. Mercalli, E. Del Grosso, G. Grosa, G. Sorba and G. C. Tron, *ChemMedChem*, 2014, **9**, 2497–2508.
12 W. Gan, X. Cao, Y. Shi and H. Gao, *J. Polym. Sci.*, 2020, **58**, 84–90.
13 I. Molina-Pinilla, K. Hakkou, L. Romero-Azogil, E. Benito, M. G. García-Martín and M. Bueno-Martínez, *Eur. Polym. J.*, 2019, **113**, 36–46.
14 J. Wu, J. Chen, J. Wang, X. Liao, M. Xie and R. Sun, *Polym. Chem.*, 2016, **7**, 633–642.
15 M. M. Obadia, A. Jourdain, P. Cassagnau, D. Montarnal and E. Drockenmuller, *Adv. Funct. Mater.*, 2017, **27**(45), 1703258.
16 M. M. Obadia, S. Fagour, Y. S. Vygodskii, F. Vidal, A. Serghei, A. S. Shaplov and E. Drockenmuller, *J. Polym. Sci., Part A: Polym. Chem.*, 2016, **54**, 2191–2199.
17 B. P. Mudraboyina, M. M. Obadia, I. Abdelhedi-Miladi, I. Allaoua and E. Drockenmuller, *Eur. Polym. J.*, 2015, **62**, 331–337.
18 L. Liu, S. He, S. Zhang, M. Zhang, M. D. Guiver and N. Li, *ACS Appl. Mater. Interfaces*, 2016, **8**, 4651–4660.
19 S. Sanghi, E. Willett, C. Versek, M. Tuominen and E. B. Coughlin, *RSC Adv.*, 2012, **2**, 848–853.
20 P. Dimitrov-Raytchev, S. Beghdadi, A. Serghei and E. Drockenmuller, *J. Polym. Sci., Part A: Polym. Chem.*, 2013, **51**, 34–38.
21 B. P. Mudraboyina, M. M. Obadia, I. Allaoua, R. Sood, A. Serghei and E. Drockenmuller, *Chem. Mater.*, 2014, **26**, 1720–1726.
22 J. M. C. Puguan, A. R. Jadhav, L. B. Boton and H. Kim, *Sol. Energy Mater. Sol. Cells*, 2018, **179**, 409–416.
23 A. Jourdain, A. Serghei and E. Drockenmuller, *ACS Macro Lett.*, 2016, **5**, 1283–1286.
24 X. Zhou, M. M. Obadia, S. R. Venna, E. A. Roth, A. Serghei, D. R. Luebke, C. Myers, Z. Chang, R. Enick, E. Drockenmuller and H. B. Nulwala, *Eur. Polym. J.*, 2016, **84**, 65–76.
25 E. M. de Souza-Fagundes, J. Delp, P. H. D. M. Prazeres, L. B. Marques, A. M. L. Carmo, P. H. F. Stroppa, N. Glanzmann, J. Kisitu, D. Szamosvàri, T. Böttcher, M. Leist and A. D. da Silva, *Chem. – Biol. Interact.*, 2018, **291**, 253–263.
26 X. Pan, L. Li, H. H. Huang, J. Wu, X. Zhou, X. Yan, J. Jia, T. Yue, Y. H. Chu and B. Yan, *J. Hazard. Mater.*, 2022, 127521.
27 J. Auwerx, *Experientia*, 1991, pp. 22–31.
28 H. Bosshart and M. Heinzelmann, *Ann. Transl. Med.*, 2016, 438.
29 G. Newbloom, S. Hoffman, A. West, M. Gile, P. Sista, H. Cheung, C. Luscombe, J. Pfaendter and L. Pozzo, *Langmuir*, 2015, **31**(1), 458–468.
30 G. Dufensne, J. Bouchard, M. Belletete, G. Durocher and M. Leclerc, *Macromolecules*, 2000, **33**(22), 8252–8257.
31 B. Kim, J.-M. Heo, M. Iqbal Khazi and J.-M. Kim, *Macromolecules*, 2021, **54**(5), 2485–2493.
32 E. Zhao, J. W. Y. Lam, L. Meng, Y. Hong, H. Deng, G. Bai, X. Huang, J. Hao and B. Z. Tang, *Macromolecules*, 2015, **48**(1), 64–71.
33 M. J. Kamlet and R. W. Taft, *J. Am. Chem. Soc.*, 1976, 377–383.

